International Journal of Power Electronics and Drive Systems (IJPEDS)
Vol. 13, No. 3, September 2022, pp. 1498~1509
ISSN: 2088-8694, DOI: 10.11591/ijpeds.v13.i3.pp1498-1509

Improved auxiliary inductive coil connectors in DC boost converters with high voltage gain for renewable energy source applications

Anusak Bilsalam[1], Nicu Bizon[2], Phatiphat Thounthong[3]
[1]Department of Electrical Engineering Technology, College of Industrial Technology (CIT), King Mongkut's University of Technology North Bangkok (KMUTNB), Bangkok, Thailand
[2]Faculty of Electronics, Communications and Computers, The University of Pitesti, Pitesti, Romania
[3]Department of Teacher Training in Electrical Engineering, Faculty of Technical Education, King Mongkut's University of Technology North Bangkok (KMUTNB), Bangkok, Thailand

Article Info

Article history:

Received Apr 26, 2022
Revised May 30, 2022
Accepted Jun 23, 2022

Keywords:

DC converter
High voltage gain
Inductive coil
Integration
Renewable energy source

ABSTRACT

This study investigates an auxiliary technique for the integration of inductive coil connectors (AIIC) within a single switched DC converter with high voltage gain for renewable energy source applications. The aim is to develop and improve the rate of voltage gain for both coils by using inductive coil connectors (coupling inductance) on the input side that goes through the ratio operator of both inductive coils of the high frequency transformer by having the prototype power circuit operate at a switching frequency 80 kHz. Experimental results show that the output power is at 125 W, output voltage is at 325 V, and input voltage is at 36 V. Furthermore, the duration of change of critical waves of the duty condition was analyzed to confirm that the results were consistent with the proposed technique.

Corresponding Author:

Anusak Bilsalam
Department of Electrical Engineering Technology, College of Industrial Technology (CIT)
King Mongkut's University of Technology North Bangkok (KMUTNB)
1518 Pracharat 1 Rd., Wongsawang, Bang sue, Bangkok 10800, Thailand
Email: anusak.b@cit.kmutnb.ac.th

1. INTRODUCTION

Boost converters are widely applied in facilities that adopt a stand-alone system, a grid-connected system, and an integrated system for generating electricity. The converter has a simple structure consisting of few devices, and it has the ability to convert direct current electricity from low voltage (12–50 V_{DC}) to high voltage (320–400 V_{DC}) [1]-[6]. In general, the factors important to improve a booster converter usually include increasing the voltage gain rate and reducing the number of devices to control the cost. Furthermore, the merits of the devices within the converters are also considered to relieve the load and stress of the electric current that originates from the power switch. Normally, to address these problems, strategies such as decreasing the amount of voltage loss and creating structures for new circuits are considered. Additionally, increasing the operating range of the duty cycle indicators will affect the rate of reverse recovery of diodes and electromag-netic interference by creating voltage stress and voltage loss, and will decrease efficiency [7]-[10]. Nonetheless, there are several other measures such as using the cascaded state (CS), switched capacitor/switched inductor (SC/SI), voltage multipliers (VMs), and voltage-lift techniques (VLs) to consider. Therefore, convertors that have high voltage gain and high voltage density will also have high incoming voltage accordingly. In addition, the voltage stress in each converter will be inversely proportional

to the output voltage of the circuit, and the current stress within the inductor will be directly proportional to the main switch [11]-[25].

In [11]-[13] cascaded state (CS) base on DC-DC converter with high conversion ratio voltage were obtained employing passive lossless clamped circuit composed of capacitors and diode is proposed circuit or cascaded state with the high step-up output voltage. As a result, the efficiency is low because the voltage stresses on the main switch and output diode of the boost converter cannot be reduced. Because their voltage gain has a quadratic topology, these converters can easily achieve a large voltage gain and greater performance. These converters may not only successfully recycle leakage energy but also effectively enhance their efficiency by utilizing the passive lossless clamped circuit. However, the switch and output diode voltage stresses keep rising, resulting in reduced efficiency and including the heat generated at each module and the amount of current in each part that disseminates electromagnetic interference. Many, switched capacitor (SC) converter basic adding several capacitors to switching-mode DC–DC converters are the topologies. The inductor's energy is utilized to charge the capacitors in series or parallel while the switch is turned off, but when the switch is turned on, the capacitors are combined in series to supply the load. However, in high-step-up applications, the component count could be quite high [14], [15].

In [16]-[18] switched inductor (SI) is a topologies similarity to proposed techniques. SI versatility allows it to be utilized in a wide range of DC–DC converters, which allows it to combine the beneficial qualities of various voltage raising techniques, as well as its simple topologies and ease of integration into any converter. By inserting a connected inductor into a non-isolated converter and selecting a suitable coupled inductor turns ratio, a non-isolated converter may be made more efficient, the voltage gain can be efficiently increased. Nevertheless, drawback these techniques by using a passive regenerative snubber circuit, on the other extreme, absorbs the energy stored in the leakage inductor, inhibits the switch voltage spike, and transmits the energy contained in the leakage inductor to the load. A dc-dc converter including combination voltage multipliers (VMs) was used to expand device or element such as active clamp switch, fast recovery diode, capacitors, and inductor tried to introduce in general backside main switch are able to give high voltage gain and recycle the leakage energy. VMs are used to bump up voltage gain, add positive traits, or help alleviate the limitations of other voltage level enhancing techniques. Nevertheless, increased power loss, voltage stress on diodes and capacitors, and circuit size may all be conse-quences of high-order multiplication and the conversion ratio is not large enough [19]-[22]. The voltage-lift methods (VLs) are an effective approach for increasing the output voltage level in high step-up converters. This procedure requires charging a capacitor to a different voltage and then stepping up the output voltage to matching the charged capacitor's voltage level or a multiple-lift circuit employing an n-stage basic diode capacitor VLs circuit was described in [23]-[25] to further rise the VLs. Furthermore, the elimination of magnetic components causes significant current spikes in switching transients. The current spikes can be decreased by increasing the parasitic electrical series resistance's (ESR) time constant and the circuit's equivalent capacitance, but this technique necessitates large capacitance values, which is the method's drawback.

In order to overcome the aforementioned drawbacks the study begins with the formulation of a new basic concept. This paper proposed topology with simplicity and a new one state provide from low voltage to high step-up output voltage, high efficiency, auxiliary technique for the integration of inductive coil connectors (AIIC) within a single switched dc converter. This paper is structured in five parts: i) concepts and techniques of the circuit as shown Figure 1; ii) concise explanation and the operating conditions; iii) design of the integration of inductive coil connector (AIIC); iv) which consists of the magnetic circuit and important parameters of the circuit explanation; and v) discuss the experimental results and the summary of the presented circuit, respectively.

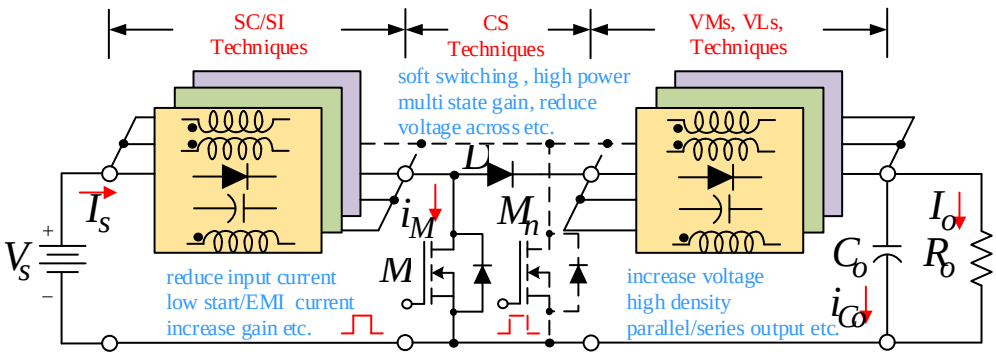

Figure 1. Guidelines conceptual circuit for high step-up conversion based on boost converter topologies

2. CIRCUIT DESCRIPTION

The auxiliary technique for the integration of inductive coil connectors in single switched converters is depicted in Figure 1. MOSFET, which is a power circuit, was used as the main switch. The connectors of inductive coils (AIIC) include two inductive coils L_1, L_2 that are products of the magnetizing inductance and the leakage inductance of each coil. For the connector between the mutual inductance M and coupling coefficient inductance ratio K, the fast-recovery diode prevents the reflux of voltage between the input and output, while the external capacitor filters the output voltage and stabilizes it, to supply the voltage to the output resistance load that connected as the front circuit of the inverter. The operating conditions of the power circuit will be separated into two modes for the following analyses and assumption.

- The power switch circuit and active/passive elements in turn on and turn off states must have ideal attributes.
- The input/output voltage must be a stable direct current.
- All inductive devices and capacitors must be large with no fluctuation of voltage and current.
- The output capacitor is large enough to maintain a consistent output voltage.

3. OPERATION MODES CIRCUIT

When the power circuit is fully operating, the shape of the time period must be consistent with the change of status in each mode, as depicted in Figures 2(a)–2(d). Operating mode I, the initial condition of the power switch is depicted in Figure 2(c). There is a supply of incoming current that goes through the first inductive coil L_1 and proceeds to the switch until it completes a cycle. Meanwhile, the first inductive coil will accumulate energy and transfer it to the second inductive coil L_2 by going through the ratio operator of both inductive coils. The amount of current that flows across the energy accumulated within the first inductive coil v_{L1} will increase linearly, and the voltage drop of the second inductive coil v_{L2} will flow out of the electrode of the inductor, passing the capacitor that was connected perpendicularly to the outgoing voltage load. Next, for this operating mode, diodes D_1 and D_2 will not induce currents. The settings of the current that flows through the inductors i_{L1} can be referred from (1).

$$i_{L1} = \frac{V_s D T_s}{L_1} \tag{1}$$

Operating mode II, in this operating mode, the power switch turn-off the current as depicted in Figure 2(d). The energy accumulated within the inductive coils L_1 and L_2 are released via the diodes D_1 and D_2, inducing a current. However, the energy from the first inductive coil does not flow through D_1 and D_2 because the second inductive coil has more energy than the first. Meanwhile, the second inductive coil releases energy to the capacitor connected perpendicularly to the outgoing voltage load. The main factor is that the current of the second inductive coil must be higher than the first inductive coil. Therefore, the voltage within the circuit of L_2 will be the parameter that decides the coordinates of the outgoing voltage of the circuit. L_1 will act as a parameter that decides the operating conditions of the circuit. The settings of the current that flows through the inductors i_{L2} can be referred from (2).

$$i_{L2} = \frac{V_s - V_o(1-D)T}{NL_2} \tag{2}$$

As N is the ratio operator of both inductive coils for the duration of the switching time period, the equation for the current of inductors 1 and 2 will be equal to zero, which can be represented as (3), for which, the output will be the rate of voltage conversion gain, represented as (4).

$$\frac{V_s DT}{N^2 L_2} + \frac{V_s - V_o(1-D)T}{NL_2} = 0 \tag{3}$$

$$\frac{V_o}{V_s} = \frac{D}{N(1-D)} + 1 \tag{4}$$

The minimum inductance of the AIIC technique can be observed and calculated from the current that flows through the minimum inductance by using the power balanced theory. The loss of passiveelements must be zero, and the magnetizing inductances that were designed based on the incoming current can be calculated from (5).

$$L_{m(min)} \approx \frac{N^2 R_o D(1-D)^2}{2f_s(N^2 + 2ND(1-D) + N^2(1-D)^2)} \tag{5}$$

Figure 3(a) (see Appendix) shows the relationship between the input voltage V_s and the output voltage V_o for various duty cycles D, and it can be seen that the voltage gain grows correspondingly as the duty cycle increases. When substitute input voltage V_s and the output voltage V_o are 36 V_{DC} and 325 V_{DC}, duty cycles D is about obtained 0.367. The relationship will be given in (19) and the voltage gain will be verified using the calculate method. Furthermore, the suggested converter has a large voltage gain while maintaining a low duty cycle. From Figure 3(b) (see Appendix), the maximum current design of main power switch to replase duty cycles D and switching frequency, then maximum current inductor is i_{Lm} =13.336 A. With reference Figure 3(c) (see Appendix), when duty cycles D is about 0.367 at fix switching frequency 80 kHz. The boundary normalized minimun inductor is obtained as 12.723 μH by (5).

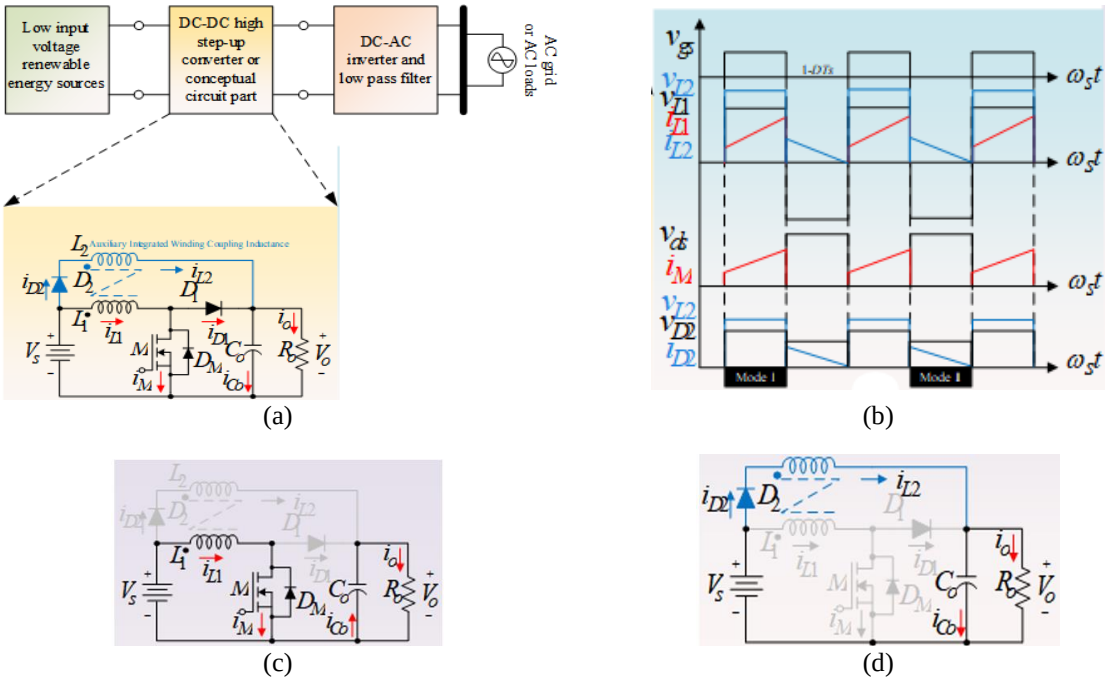

Figure 2. The proposed power converter state and operating concept (a) proposed AIIC converter, (b) key waveforms, (c) operating mode I, and (d) operating mode II

4. DESIGN MAGNETIC AND POWER STATE CIRCUIT

The design process begins by first designing the magnetic circuit to assess the power circuit depicted in Figure 4(a). The steps in the process are mentioned:

- Choose the size and type of the iron core and set the magnetic resistance of each part $\Re_1$- $\Re_9$
- Find the equivalent magnetizing resistance $\Re$.
- Find are both magnetizing inductance L_1 and L_2.
- Find the coupling coefficient inductance ratio of each coil K_1, K_2 and all performance coefficient factor K.
- Find the turn ratio a from AIIC technique.
- Assess the subparts of the power circuit by deciding the output voltage V_o and the output power P_o to determine the DC side load resistance.
- Find are maximum current of power switch i_{Lmax} the value of the output capacitor C_o and choose the ripple output to be less than 1%.
- Finally, calculate the loss of each part such as power switch P_{rds}, the power loss in each diode P_{D1}, P_{D2}, the conduction loss in both inductors P_{rL1} and P_{rL2}.

4.1. Magnetic design AIIC technique

The assessment of each magnetizing resistance is very important to the power circuit because the parameters that were calculated can be used to find the value of the inductor of each coil L_1, L_2. The coupling coefficient inductance ratio K and the number of rounds of the inductor will be calculated from the length and area depicted in Figures 4(a)–4(c). The magnetizing resistance can be separated into (6) and (7). The magnetizing resistance air gap are calculation divided as (8) and (9).

$$\Re_1 = \frac{l_{C1}}{\mu_r \mu_o A_{C1}} = \frac{30\times10^{-3}}{1690\times4\pi\times10^{-7}\times90\times10^{-6}} = 0.156\times10^6 AT/\text{Wb} \quad (6)$$

$$\Re_3 = \frac{l_{C2}}{\mu_r \mu_o A_{C2}} = \frac{15\times10^{-3}}{1690\times4\pi\times10^{-7}\times180\times10^{-6}} = 0.039\times10^6 AT/Wb \quad (7)$$

$$\Re_4 = \frac{l_g}{\mu_o A_{g1}} = \frac{0.46\times10^{-3}}{4\pi\times10^{-7}\times90\times10^{-6}} = 2.917\times10^6 AT/\text{Wb} \quad (8)$$

$$\Re_5 = \frac{l_g}{\mu_o A_{g1}} = \frac{0.64\times10^{-3}}{4\pi\times10^{-7}\times180\times10^{-6}} = 2.829\times10^6 AT/\text{Wb} \quad (9)$$

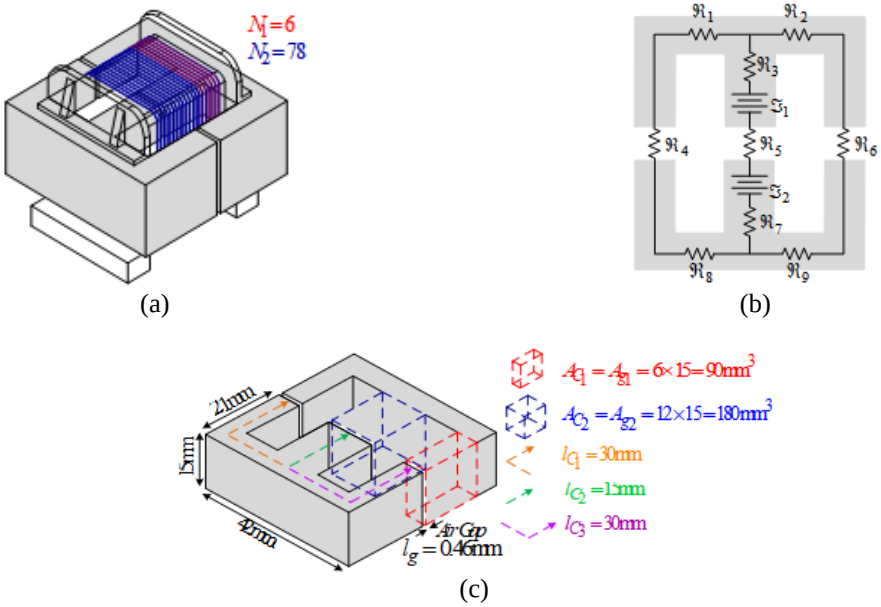

Figure 4. Photograph of integrated auxiliary winding coupling inductance technique (AIIC) of the proposed converter (a) oblique photograph with the consist of main inductor N_1 and auxiliary wining coupling inductor N_2; (b) equivalent circuit of a magnetizing resistance in a sub cross section each of area; and (c) cross section photograph and areas of a ferromagnetic core

The constant of the special attribute of ferrite cores EE42/N87 consists of the relative permittivity of the material, which equals to 1690, and the permeability of a vacuum, which equals to 4π×10-7 H/m. According to the calculation, the value of the external rim of the core of the magnetizing resistance equals to $\Re_1=\Re_2=\Re_8=\Re_9$, value of the central area within the magnetizing resistance equals to $\Re_3=\Re_7$, values of the sides of the magnetizing resistance that was the vacuum equals to $\Re_4=\Re_6$, and internal values of the magnetizing resistance of the air gap $\Re_5$. Therefore, the magnetizing resistance can be calculated as (10). The value of both coils can be explained by (11) and (12).

$$\Re_t = (\Re_3 + \Re_7 + \Re_5) = (0.0039\times10^6 \times 0.0039\times10^6 \times 2.829\times10^6) = 2.907\times10^6 AT/\text{Wb} \quad (10)$$

$$L_1 = \frac{{N_1}^2}{\Re_t} = \frac{6^2}{2.097\times10^6} = 23.416\,\mu H \quad (11)$$

$$L_2 = \frac{{N_2}^2}{\Re_t} = \frac{78^2}{2.097\times10^6} = 2.092\ \text{mH} \quad (12)$$

The next step is to evaluate the measurement of the leakage inductor from the test stand by using the short circuit test, for which the value of the leakage inductor L_{lk1}, L_{lk2} is equal to 1.348 µH and 118.027 µH. Retest the magnetizing inductance of both coils from the design. This can be explained by (13) and (14).

$$L_{m1} = L_1 - L_{lk1} = (12.383\times10^{-6}) - (1.348\times10^{-6}) = 11.035\,\mu H \quad (13)$$

$$L_{m2} = L_2 - L_{lk2} = (3.957 \times 10^{-3}) - (118.027 \times 10^{-6}) = 1.973 \text{ mH} \quad (14)$$

Next, the ability of each coupling coefficient inductance K_1, K_2 is assessed by (15) and (16).

$$K_1 = \frac{L_{m1}}{L_1} = \frac{11.035 \times 10^{-6}}{12.383 \times 10^{-6}} = 0.891 \quad (15)$$

$$K_2 = \frac{L_{m2}}{L_2} = \frac{1.973 \times 10^{-3}}{2.092 \times 10^{-3}} = 0.943 \quad (16)$$

For easier understanding, the ability of the coupling coefficient inductance ratio of all coils K can be calculated by substituting (15) and (16) in (17).

$$K = \sqrt{K_1 K_2} = \sqrt{0.891 \times 0.943} = 0.956 \quad (17)$$

In conclusion, for the ratio operator of the connector of the inductor of the AIIC technique, the magnetic circuit can confirm that (18).

$$N = \sqrt{K_1 / K_2} \times \sqrt{L_1 / L_2} = \sqrt{0.891 / 0.943} \times \sqrt{(12.383 \times 10^{-6}) / (2.092 \times 10^{-3})} = 0.0723 \quad (18)$$

4.2. Power state design

The power state design can be separated into to two parts: designing the circuit's parameters and calculating the subparts of electric power loss of each device, as well as the aggregate loss. The calculation will be based on the analysis of the steady state at the switch frequency of 80 kHz, incoming voltage of 36 V_{DC}, and outgoing voltage of 325 V_{DC} at 125 W of electric power, for which the outgoing electrical resistance is $R_o = V_o^2/P_o$ = 845 Ω at full electric power. Therefore, the duty cycle will be (19).

$$D = \frac{V_o - V_s}{V_s\left(\frac{1}{N} - 1\right) + V_o} = \frac{325 - 36}{36\left(\frac{1}{0.0723} - 1\right) + 325} = 0.367 \quad (19)$$

According to (5), the minimum inductance will be 12.723 μH to place the circuit into the continues conduction mode. For practicality, the smaller inductor will be L_1 =13.6 μH, and the outgoing capacitor used to stabilize the voltage with a ripple voltage ratio that is less than 1% can be obtained from the equation $C_o = (1\text{-}D)/8L_1(\Delta V_o / V_o)f_s^2$=47 μF. Based on the calculation, the size of the outgoing capacitor will be a standard size of 100 µF/400 V, for which the parameters were plotted on a relativity graph as depicted in Figures 3(a)–3(c).

4.3. Power loss design

This important calculation is used to find the amount of loss from the power conduction of each circuit, which could occur in the auxiliary device for the AIIC technique and the active/passive element of the circuit. This study uses MOSFET No. IRFP4332PBF with an inductive resistance value of r_{ds}=29 mΩ, along with the MUR 840 and MUR 8100, which are fast recovery diodes that have a forward voltage drop when the current inductance equals to 1.28 and 1.8 V, respectively. The current that runs through the switch i_M is calculated using the equation from maximum current inductor i_{Lm1}. Therefore, the loss of each part can be calculated separately as:

$$P_{rds} = (i_M)^2 rds/2 = (13.332)^2 \times 29 \times 10^{-3}/2 = 2.577W \quad (20)$$

$$P_{D1} = \frac{V_{FD1} P_o}{V_o} = \frac{1.28 \times 125}{325} = 0.492W \quad (21)$$

$$P_{D2} = \frac{V_{FD2} P_o}{V_o} = \frac{1.8 \times 125}{325} = 0.692W \quad (22)$$

The electrical parasitic series resistance r_p, r_s of both coils will be equal to 0.038 Ω and 4.18 Ω, which were derived from the LCR meter, which is a measurement tool that measures loss in inductors by calculating the maximum current of the magnetizing inductor, which can be explained by $i_{Lm} = V_s D/f_s L_{m(\min)}$ = 13.332 A. Therefore, the loss of each part can be calculated by (23) and (24).

$$P_{rL1} = (i_{Lm})^2 r_{L1} = (13.332)^2 \times 0.038 = 6.754W \quad (23)$$

$$P_{rL2} = \left(I_o\sqrt{2}\right)^2 r_{L2} = (0.537)^2 \times 4.18 = 1.205W \quad (24)$$

Finally, the loss of each part can be combined to find the overall performance value of the circuit as (25). The extent of the equivalent circuit and the relationship between breakdown power loss are depicted in Figures 5(a) and 5(b).

$$\eta = \frac{P_o}{P_o+(P_{rds}+P_{D1}+P_{D2}+P_{rL1}+P_{rL2})} = 0.914 \quad (25)$$

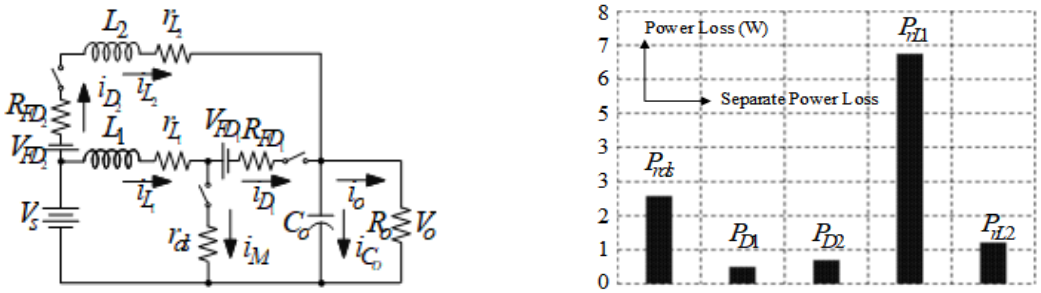

(a) (b)

Figure 5. Analysis and relationship of proposed circuit (a) equivalent circuit for the conduction loss and (b) relationship bar graph breakdown of the overall conduction loss

5. SIMULATION AND EXPERIMENTAL RESULTS

A prototype of the AIIC was simulated and implemented within a single switched dc converter with significant voltage gain. The topology parameters presented in Table 1 were used in the simulation and implementation. The switching frequency was set to be around 80 kHz. The overall simulation results are shown in Figures 6(a)-6(d). The 36 V_{DC} input voltage was supplied from a series-parallel battery pack with the constant voltage. Figure 6(a) depicts the simulated voltage, current, and power input waveforms. The waveform drain–source voltage across v_{ds}, current pass of main power switch I_M and current pass inductor i_{L1} and then power switch was operated under zero turn-on, as shown in Figure 6(b), The investigates operation continuous conduction mode CCM of an auxiliary coupling technique from voltage and current both inductors as shown in Figure 6(c). The last simulated of the output voltage, current, and output power waveforms are shown in Figure 6(d).

Table 1. Utilized component and parameter of prototype

Parameter	Symbol	Value/part number	Type
Input voltage	V_i	36 V_{DC}	-
Output voltage	V_o	325 V_{DC}	-
Output power	P_o	125 W	-
Output capacitor	C_o	0.33 μF	Electrolyte/400 V
Switching frequency	f_s	80 kHz	SG3525 Gate Driven
Power MOSFETs	M	IRFP4332PBF	N-Chanel MOSFETs, V_{DSS}=250 V, I_D=57 A, $R_{DS\,(on)}$=29 mΩ
Fast recovery diode	D_1	MUR 840	Fast-recovery diode, V_{RRM}=400 V, $I_{F(AV)}$=8 A, V_F=1.28 V
Fast recovery diode	D_2	MUR 8100	Fast-recovery diode, V_{RRM}=1000 V, $I_{F(AV)}$=8 A, V_F=1.8 V
Inductance	L_1, L_2	13.6 µH, 3.920 mH	EE42/13/7 N87-EPCOS, L_1= (6 Turn), L_2= (72 Turn)
Leakage inductance	L_{lk1}, L_{lk2}	1.348 µH, 118.027 µH	EE42/13/7 N87-EPCOS
Magnetizing inductance	L_{m1}, L_{m2}	11.305 µH, 1.973 mH	EE42/13/7 N87-EPCOS
Electrical parasitic Series resistance	r_p, r_s	0.146 Ω, 9.18 Ω	EE42/13/7 N87-EPCOS
Switching frequency	f_s	80 kHz	-
Operating mode	-	CCM	Continuous conduction mode

The discussion results of the experiment are shown in Figures 7(a)-7(d). At a power input of 137 W, the voltage, current, and power input were measured, as shown in Figure 7(a). The voltage and current waveforms of MOSFET M is shown in Figure 7(b). The switches indicating that they operated under zero turn-on condition. High-frequency square-wave voltage is represented by the voltage across the waveform on both inductors, whereas current pass inductors has operated continuous conduction mode are shown in Figure 6(c). The voltage, current, and power waveforms measured at the output side have a highest value of 125 W, as shown in Figure 7(c). The investigate route power loss of voltage across v_{L1} and current waveform i_{L1} of the inductor in the path of loss because of auxiliary component in the prototype are shown Figures 8(a) and 8(b). The power loss is also low because auxiliary technique for the integration of inductive coil, which it non

absorbs energy in during turn-on and turn off. In this section discussion comparison of previously proposed high step-up converters and their relevant publications. is shown Tables 2.

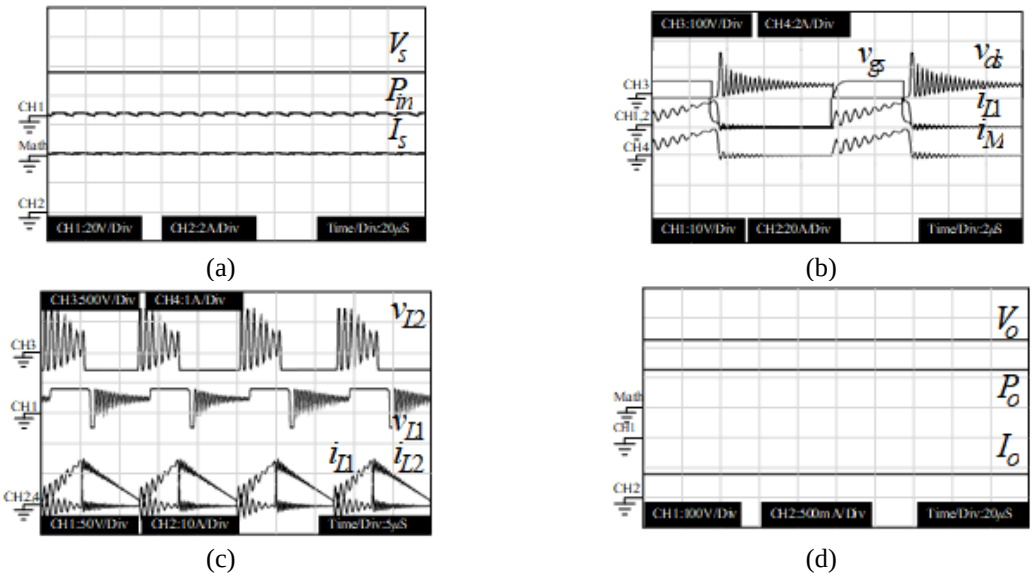

Figure 6. Simulation result of the proposed circuit (a) voltage V_s, current I_s, and power P_s waveforms at the input side; (b) voltage gate driven v_{gs}, drain–source voltage across v_{ds}, current power switch i_M and current on inductor i_{L1}; (c) voltage across v_{L1}, v_{L2} and current of a both high frequency inductors i_{L1}, i_{L2}; and (d) voltage V_o, current I_o, and power P_o waveforms at the output side

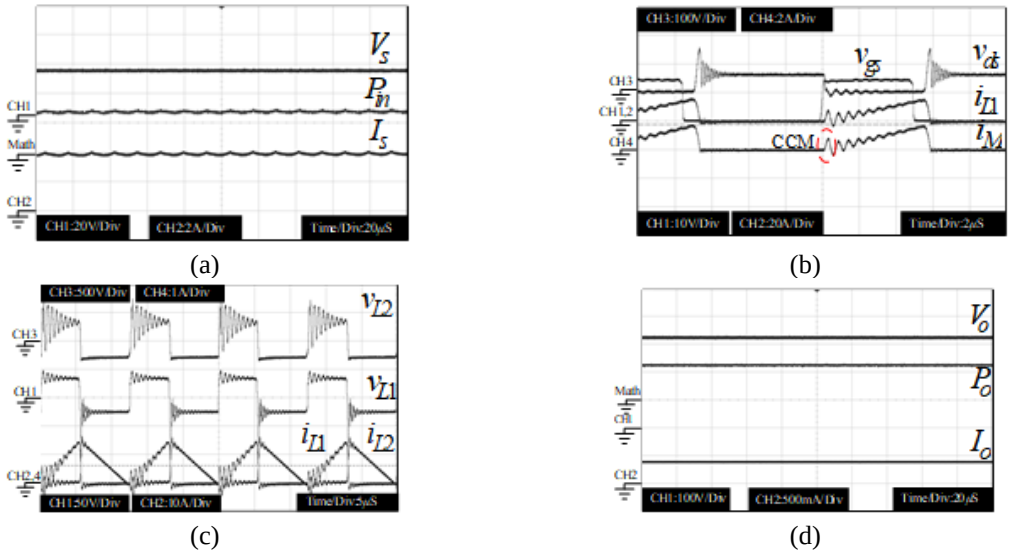

Figure 7. Experimental result of the proposed circuit (a) voltage V_s, current I_s, and power P_s waveforms at the input side; (b) voltage gate driven v_{gs}, drain–source voltage across v_{ds}, current power switch i_M and current on inductor i_{L1}; (c) voltage across v_{L1}, v_{L2} and current of a both high frequency inductors i_{L1}, i_{L2}; and (d) voltage V_o, current I_o, and power P_o waveforms at the output side

Last, discussion power loss each in Figures 5 (a) and (b), equivalent circuit for the conduction loss analysis and overall breakdown of the AIIC with dc converter circuit is given as follows. The most significant lose are those that occur on inductor L_1 and main power switch eques of 6.754 and 2.577 W. the losses, which amount to 4.92 and 1.88 % in this section, can be calculation 6.80 %. The loss inductor L_2 and both fast recovery power diode eques were 1.205, 0.492, and 0.692 W, with losses from component of 0.87, 0.35, and 0.50 %, respectively. Table 3 summarizes the outcomes of the simulations and experiments. The

output voltage of the simulation result case is 355 V_{DC}, which is more than the implement result equal to 325 V_{DC} and overall measure values of the proposed circuit as shown Table 3. In addition, Figure 9(a) shows the regulation of the output voltage when the output power was 50 to 150 W. The minimum and maximum output voltage are eques to 325-350 V_{DC}, when change output power at 50-125 W following stand MIC condition (320≤Vo≤400 V_{DC}). The measured efficiency of the AIIC dc converter was approximately 92% at the full load condition, and the maximum efficiency was 94% at approximately 140 W. The overall efficiency, output voltage, and output power relationship parameters, as well as the prototype circuit are shown in Figures 9(a) and 9(b).

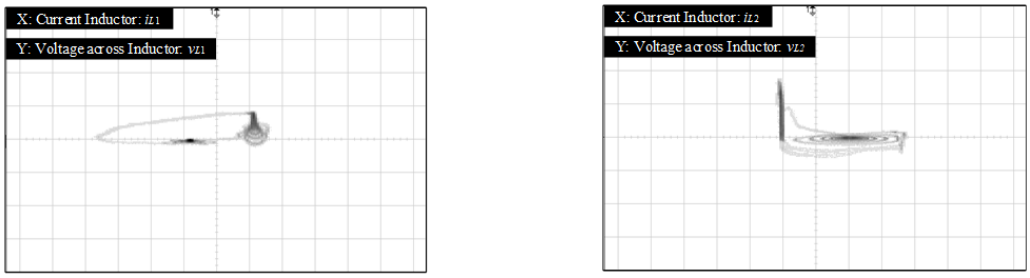

(a) (b)

Figure 8. Experimental result of power loss (a) relationship power loss of route inductor L_1 voltage across v_{L1}v and current waveform i_{L1} and (b) relationship power loss of route inductor L_2 voltage across v_{L2}v and current waveform i_{L2}

Table 2. Performance comparison between the proposed converter and high step-up converter topologies

No. of ref	No. of component					Range	Conversion ratio	Minimum inductance	Operation
	Sw	D	L	C	Core	I/O voltage	(V_o/V_i)	(L_{min})	mode/size
Ref. [12]	1	5	4	4	3	38/400 V	$\frac{1+ND}{(1-D)^2}$	$\frac{V_{in}D}{(1-D)\Delta I_{Lm}f_s}$	CCM/ Middle
Ref. [15]	2	2	3	4	4	40-400 V	$\frac{1+N}{(1-D)^2}$	$\frac{V_{in}(V_o-(N+2)V_{in})}{0.25I_Lf_sV_o}$	CCM/ Middle
Ref. [18]	1	4	2	4	1	20/400 V	$\frac{1+(1+D)N}{1-D}$	$\frac{V_{in}DT_s}{I_{Lmp}}$	CCM/ Large
Ref. [19]	1	3	2	3	2	12/100 V	$\frac{2}{1-D}$	$\frac{V_{in}D}{\Delta I_Lf_s}$	CCM/ Large
Ref. [20]	1	4	2	4	1	40/400 V	$\frac{2+N+ND}{1-D}$	$\frac{DV_{in}}{L_mf_s}$	CCM/ Large
Ref. [21]	1	3	3	4	1	36/380 V	$\frac{N+2}{1-D}$	$\frac{V_{in}D}{\Delta I_{Lf}f_s}$	CCM/ Large
Ref. [23]	2	4	4	4	2	40/380 V	$\frac{2N+2}{1-D}$	$\frac{5V_{in}D}{\Delta I_{in}f_s}$	CCM/ Large
Ref. [25]	2	7	3	7	1	32/800 V	$\frac{2(N+2)}{1-D}$	$\frac{DV_{in}}{f_s\Delta I_{Lm}}$	CCM/ Large
Proposed	1	2	2	1	1	36/325 V	$\frac{D}{N(1-D)}+1$	$\frac{N^2R_oD(1-D)^2}{2f_s(D^2+2ND(1-D)+N^2(1-D)^2)}$	CCM /Small

Table 3. Comparison of the prototype's parameter simulation and experimental results

Section	Parameter	Symbol	Simulation	Experimental	Detail
Input side	input voltage	V_{in}	36 V	36 V	average value
	input current	I_{in}	3.80 A	3.82 A	average value
	input power	P_{in}	136 W	137 W	average value
High frequency and equipment semi-conductor device	gate driven signal	v_{qs}	15 V	15 V	peak value
	voltage across power switch	v_{ds}	157.3 V	156.0 V	peak value
	current of power switch	i_m	14 A	14.8 A	peak value
	voltage across both inductors	$v_{L1,}v_{L2}$	36 V, 323 V	36 V, 325 V	rms value
	current on both inductors	$i_{L1,}i_{L2}$	14 A, 1.52 A	14 A, 1.67 A	peak value
	voltage across both power diode	$v_{D1,}v_{D2}$	335 V, 1.27 kV	335 V, 1.31 kV	peak value
	current on both power diode	$i_{D1,}i_{D2}$	0.15 A, 1.7 A	0.15 A, 1.92 A	peak value
Output side	output voltage	V_o	330 V	325 V	average value
	output current	I_o	378 mA	385 mA	average value
	output power	V_o	125 W	125 W	average value
	efficiency	η	91.72	91.33	percentage

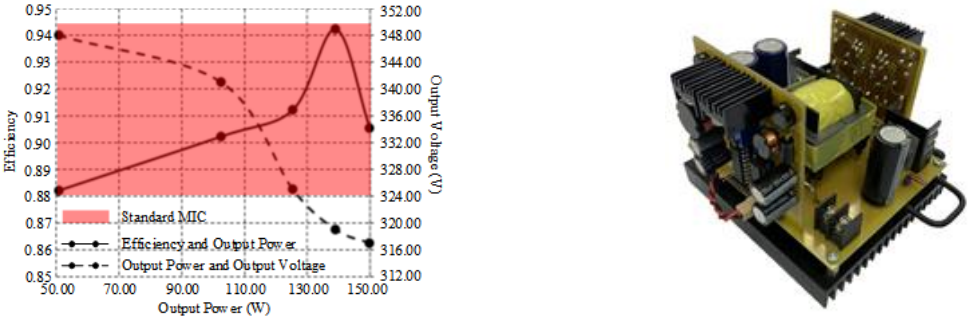

Figure 9. Experimental results of the relationship graph and photograph (a) relationship between the efficiency and output power P_o and output voltage V_o and (b) prototype photograph of the proposed circuit

6. CONCLUSION

This paper presented by using the auxiliary technique for the integration of inductive coil connectors in single switched dc converters to increase voltage gain ratio, the circuit receives an input voltage of 36 V_{DC} for the conversion of direct current on the high side output at 325 V_{DC} and 125 W. Once it operates at 80 kHz, the overall performance is 91.5% at full load. The operating range of the duty cycle did not exceed 0.5 (D≤0.5) when the voltage gain ratio was high, which is consistent with the objective of this study. The advantages of using this method are as follows: high voltage gain conversion ratio, less components and low cost in the system, easily simplify design parameter in the circuit provide equivalent magnetic circuit and main idea concept proposed can be inductive coil connectors (AIIC) within applied to non-isolated conversional dc to dc converter topologies. Nonetheless, a problem was found that there was a voltage drop across diode D_2. The technique still produces high voltage that could be reduced by using an active semiconductor power switch. According to the assessment and overall calculation, the proposed circuit is suitable to by applied for stand-alone, grid-connected, and hybrid micro renewable systems and used for high voltage gain converters.

ACKNOWLEDGEMENTS

This work was supported in part by an International Research Partnership "Electrical Engineering–Thai French Research Center (EE-TFRC)" under the project framework of the Lorraine Université d'Excellence (LUE) in cooperation between Université de Lorraine and King Mongkut's University of Technology North Bangkok and in part by the National Research Council of Thailand (NRCT) under Senior Research Scholar Program under Grant No. N42A640328 and main supported by King Mongkut's University of Technology North Bangkok (Grant No. Res-CIT0280/2021).

APPENDIX

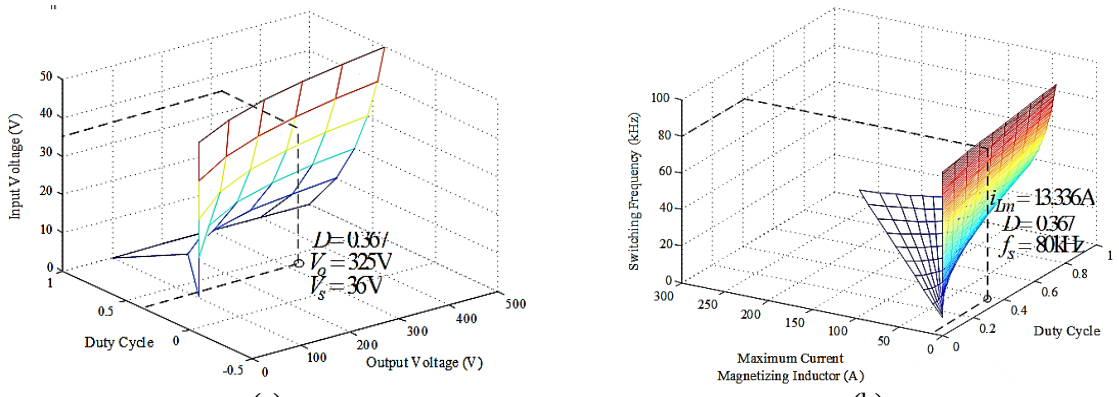

Figure 3. Relationships graphs parameter: (a) relationships between input voltage V_s and duty cycle D and output voltage V_o; and (b) relationships between switching frequency f_s and maximum current magnetizing inductor i_{Lmax} and duty cycle D

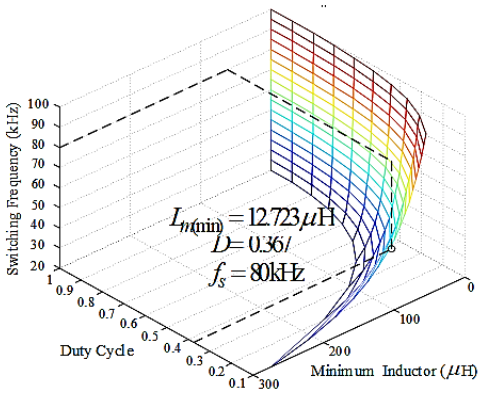

(c)

Figure 3. Relationships graphs parameter: (c) relationships between switching frequency f_s and and duty cycle D and minimum inductor $L_{m(min)}$ (continue)

REFERENCES

[1] S. B. Kjaer, J. K. Pedersen, and F. Blaabjerg, "A review of single-phase grid-connected inverters for photovoltaic modules," in *IEEE Transactions on Industry Applications*, vol. 41, no. 5, pp. 1292-1306, 2005, doi: 10.1109/TIA.2005.853371.

[2] P. Thounthong, B. Davat, S. Rael, and P. Sethakul, "Fuel cell high-power applications," in *IEEE Industrial Electronics Magazine*, vol. 3, no. 1, pp. 32-46, Mar. 2009, doi: 10.1109/MIE.2008.930365.

[3] W. Li and X. He, "Review of nonisolated high-step-up DC/DC converters in photovoltaic grid-connected applications," in *IEEE Transactions on Industrial Electronics*, vol. 58, no. 4, pp. 1239-1250, Apr. 2011, doi: 10.1109/TIE.2010.2049715.

[4] M. Forouzesh, Y. P. Siwakoti, S. A. Gorji, F. Blaabjerg, and B. Lehman, "Step-up DC–DC converters: a comprehensive review of voltage-boosting techniques, topologies, and applications," in *IEEE Transactions on Power Electronics*, vol. 32, no. 12, pp. 9143-9178, Dec. 2017, doi: 10.1109/TPEL.2017.2652318.

[5] E. Romero-Cadaval, B. Francois, M. Malinowski, and Q. -C. Zhong, "Grid-connected photovoltaic plants: an alternative energy source, replacing conventional sources," in *IEEE Industrial Electronics Magazine*, vol. 9, no. 1, pp. 18-32, Mar. 2015, doi: 10.1109/MIE.2014.2362211.

[6] S. Kouro, J. I. Leon, D. Vinnikov, and L. G. Franquelo, "Grid-connected photovoltaic systems: an overview of recent research and emerging PV converter technology," in *IEEE Industrial Electronics Magazine*, vol. 9, no. 1, pp. 47-61, Mar. 2015, doi: 10.1109/MIE.2014.2376976.

[7] H. Liu, H. Hu, H. Wu, Y. Xing, and I. Batarseh, "Overview of high-step-up coupled-inductor boost converters," in *IEEE Journal of Emerging and Selected Topics in Power Electronics*, vol. 4, no. 2, pp. 689-704, Jun. 2016, doi: 10.1109/JESTPE.2016.2532930.

[8] L. Schmitz, D. C. Martins, and R. F. Coelho, "Comprehensive conception of high step-up DC–DC converters with coupled inductor and voltage multipliers techniques," in *IEEE Transactions on Circuits and Systems I: Regular Papers*, vol. 67, no. 6, pp. 2140-2151, Jun. 2020, doi: 10.1109/TCSI.2020.2973154.

[9] Y. J. A. Alcazar, D. de Souza Oliveira, F. L. Tofoli, and R. P. Torrico-Bascopé, "DC–DC nonisolated boost converter based on the three-state switching cell and voltage multiplier cells," in *IEEE Transactions on Industrial Electronics*, vol. 60, no. 10, pp. 4438-4449, Oct. 2013, doi: 10.1109/TIE.2012.2213555.

[10] S. Chen *et al*., "Research on topology of the high step-up boost converter with coupled inductor," in *IEEE Transactions on Power Electronics*, vol. 34, no. 11, pp. 10733-10745, Nov. 2019, doi: 10.1109/TPEL.2019.2897871.

[11] J. Ai, M. Lin, and M. Yin, "A family of high step-up cascade DC–DC converters with clamped circuits," in *IEEE Transactions on Power Electronics*, vol. 35, no. 5, pp. 4819-4834, May 2020, doi: 10.1109/TPEL.2019.2943502.

[12] S. Lee and H. Do, "High step-up coupled-inductor cascade boost DC–DC converter with lossless passive snubber," in *IEEE Transactions on Industrial Electronics*, vol. 65, no. 10, pp. 7753-7761, Oct. 2018, doi: 10.1109/TIE.2018.2803731.

[13] Y. Wang, Y. Qiu, Q. Bian, Y. Guan, and D. Xu, "A single switch quadratic boost high step up DC–DC converter," in *IEEE Transactions on Industrial Electronics*, vol. 66, no. 6, pp. 4387-4397, Jun. 2019, doi: 10.1109/TIE.2018.2860550.

[14] G. Wu, X. Ruan, and Z. Ye, "Nonisolated high step-up DC–DC converters adopting switched-capacitor cell," in *IEEE Transactions on Industrial Electronics*, vol. 62, no. 1, pp. 383-393, Jan. 2015, doi: 10.1109/TIE.2014.2327000.

[15] Y. Zheng, B. Brown, W. Xie, S. Li, and K. Smedley, "High step-up DC–DC converter with zero voltage switching and low input current ripple," in *IEEE Transactions on Power Electronics*, vol. 35, no. 9, pp. 9416-9429, Sep. 2020, doi: 10.1109/TPEL.2020.2968613.

[16] Rong-Jong Wai and Rou-Yong Duan, "High step-up converter with coupled-inductor," in *IEEE Transactions on Power Electronics*, vol. 20, no. 5, pp. 1025-1035, Sep. 2005, doi: 10.1109/TPEL.2005.854023.

[17] S. Changchien, T. Liang, J. Chen, and L. Yang, "Novel high step-up DC–DC converter for fuel cell energy conversion system," in *IEEE Transactions on Industrial Electronics*, vol. 57, no. 6, pp. 2007-2017, Jun. 2010, doi: 10.1109/TIE.2009.2026364.

[18] W. Li and X. He, "A family of interleaved DC–DC converters deduced from a basic cell with winding-cross-coupledinductors (WCCIs) for high step-upor step-down conversions," in *IEEE Transactions on Power Electronics*, vol. 23, no. 4, pp. 1791-1801, Jul. 2008, doi: 10.1109/TPEL.2008.925204.

[19] M. Prudente, L. L. Pfitscher, G. Emmendoerfer, E. F. Romaneli, and R. Gules, "Voltage multiplier cells applied to non-isolated DC–DC converters," in *IEEE Transactions on Power Electronics*, vol. 23, no. 2, pp. 871-887, Mar. 2008, doi: 10.1109/TPEL.2007.915762.

[20] A. Ajami, H. Ardi, and A. Farakhor, "A novel high step-up DC/DC converter based on integrating coupled inductor and switched-capacitor techniques for renewable energy applications," in *IEEE Transactions on Power Electronics*, vol. 30, no. 8, pp. 4255-4263, Aug. 2015, doi: 10.1109/TPEL.2014.2360495.
[21] Y. Deng, Q. Rong, W. Li, Y. Zhao, J. Shi, and X. He, "Single-switch high step-up converters with built-in transformer voltage multiplier cell," in *IEEE Transactions on Power Electronics*, vol. 27, no. 8, pp. 3557-3567, Aug. 2012, doi: 10.1109/TPEL.2012.2183620.
[22] J. Ai and M. Lin, "Ultralarge gain step-up coupled-inductor DC–DC converter with an asymmetric voltage multiplier network for a sustainable energy system," in *IEEE Transactions on Power Electronics*, vol. 32, no. 9, pp. 6896-6903, Sep. 2017, doi: 10.1109/TPEL.2016.2626383.
[23] S. -W. Seo, D. -K. Lim, and H. H. Choi, "High step-up interleaved converter mixed with magnetic coupling and voltage lift," in *IEEE Access*, vol. 8, pp. 72768-72780, 2020, doi: 10.1109/ACCESS.2020.2983757.
[24] T. Liang, J. Lee, S. Chen, J. Chen, and L. Yang, "Novel isolated high-step-up DC–DC converter with voltage lift," in *IEEE Transactions on Industrial Electronics*, vol. 60, no. 4, pp. 1483-1491, Apr. 2013, doi: 10.1109/TIE.2011.2177789.
[25] M. L. Alghaythi, R. M. O'Connell, N. E. Islam, M. M. S. Khan, and J. M. Guerrero, "A high step-up interleaved DC-DC converter with voltage multiplier and coupled inductors for renewable energy systems," in *IEEE Access*, vol. 8, pp. 123165-123174, 2020, doi: 10.1109/ACCESS.2020.3007137.

BIOGRAPHIES OF AUTHORS

Anusak Bilsalam (Member, IEEE) was born in Nakhon Si Thammarat, Thailand. He received the B.Ind.Tech. degree in power electronics technology from the King Mongkut's Institute of Technology North Bangkok (KMITNB), Bangkok, Thailand, in 2004, the M.E. degree in electrical engineering from the King Mongkut's University of Technology Thonburi (KMUTT), Bangkok, in 2010, and the Ph.D. degree in electrical engineering from the King Mongkut's University of Technology North Bangkok (KMUTNB), in 2015. From 2013 to 2017, he was a lecturer with the Division of Energy Technology and Management, Faculty of Science, Energy and Environment, King Mongkut's University of Technology North Bangkok (Rayong campus). He is currently an Assistant Professor with the Department of Electrical Engineering Technology, College of Industrial Technology (CIT), KMUTNB. His research interests include high-frequency and efficiency switching power converter, zero voltage and zero current switching techniques in resonant converter, math model of a photovoltaic cells and renewable energy system and induction/dielectric heating application. He can be contacted at email: anusak.b@cit.kmutnb.ac.th.

Nicu Bizon (Senior Member, IEEE) was born in Albesti de Muscel, Arges county, Romania, in 1961. He received the B.S. degree in electronic engineering and the Ph.D. degree in automatic systems and control from the University "Polytechnic" of Bucharest, Bucharest, Romania, in 1986 and 1996, respectively. From 1996 to 1989, he was in Hardware Design with Dacia Renault SA, Pite¸sti, Romania. He is currently a Professor with The University of Pitesti, Pite¸sti. He is an Editor of ten books and more than 500 articles in scientific fields related to energy (from these 115 articles are indexed in WOS (39 Q1; 2 Q2; 2 Q3; 2 Q4; 56 in conferences; and 21 chapters); and *H*-index WOS = 21). His current research interests include power electronic converters, fuel cell and electric vehicles, renewable energy, energy storage system, microgrids, and control and optimization of these systems. Dr. Bizon received two awards from the Romanian Academy, in 2013 and 2016. He can be contacted at email: nicu.bizon@upit.ro.

Phatiphat Thounthong (Senior Member, IEEE) was born in Phatthalung, Thailand, on December 29, 1974. He received the B.S. and M.E. degrees in electrical engineering from King Mongkut's Institute of Technology North Bangkok (KMITNB), Bangkok, Thailand, in 1996 and 2001, respectively, the Ph.D. degree in electrical engineering from Institut National Polytechnique de Lorraine (INPL), Nancy-Lorraine, France, in 2005, and the Habilitation à Diriger la Recherche (HDR) from Université de Lorraine, Nancy-Lorraine, France in 2020. Since 2012, he has been a Full Professor in the Department of Teacher Training in Electrical Engineering, King Mongkut's University of Technology North Bangkok. He is the author of 231 scientific papers (including 21 papers in IEEE Transactions/Magazines) published in Scopus with citations=4,746 times and h-index=34. His current research interests include power electronics, electric drives, electric vehicles, electrical devices (fuel cells, photovoltaic, wind turbine, batteries and supercapacitors, nonlinear controls and observers. He can be contacted at email: phatiphat.t@fte.kmutnb.ac.th.